JPCCCK

OCTOBER 28, 2010
VOLUME 114
NUMBER 42

pubs.acs.org/JPCC

THE JOURNAL OF PHYSICAL CHEMISTRY C

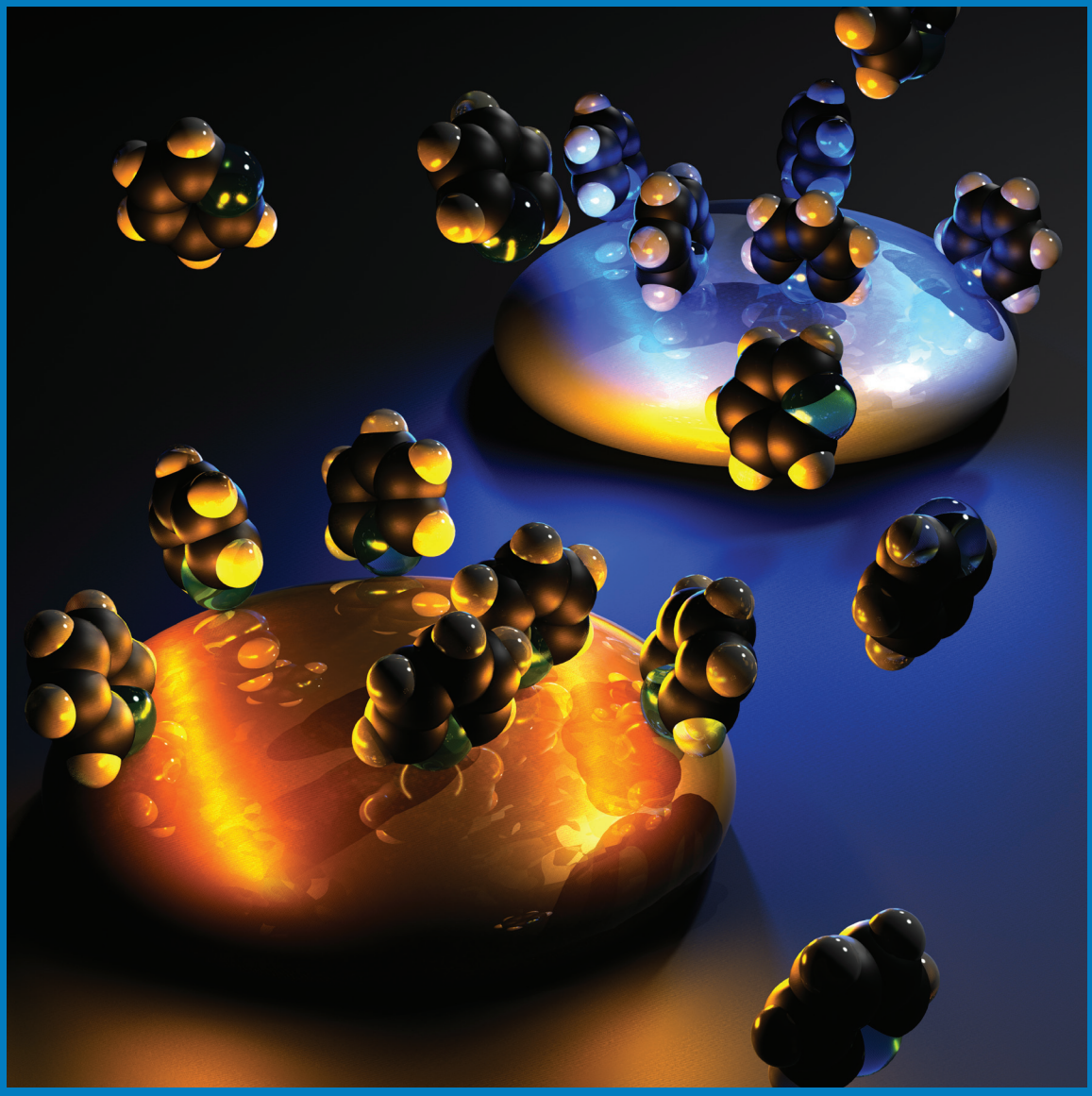

Effects of Intrinsic Fano Interference on SERS Performances of Platinum and Gold (see page XA)

NANOMATERIALS, INTERFACES, HARD MATTER

ACS Publications
High quality. High impact.

www.acs.org

Effects of Intrinsic Fano Interference on Surface Enhanced Raman Spectroscopy: Comparison between Platinum and Gold

Qingzhen Hao,[†,‡] Bala Krishna Juluri,[‡] Yue Bing Zheng,[‡] Bei Wang,[†] I-Kao Chiang,[‡] Lasse Jensen,[§] Vincent Crespi,[†,∥] Peter C. Eklund,[†,∥] and Tony Jun Huang*[,‡]

Department of Physics, Department of Engineering Science and Mechanics, Department of Chemistry, and Department of Materials Science and Engineering, The Pennsylvania State University, University Park, Pennsylvania 16802

Received: June 8, 2010; Revised Manuscript Received: July 29, 2010

Using pyridine as a probe molecule, we performed surface enhanced Raman spectroscopy (SERS) studies on platinum and gold nanodisk arrays at both plasmon resonant and off-plasmon resonant excitation wavelengths. A large Raman cross-section enhancement factor (EF) of $\sim 10^6$ was obtained with plasmon resonant excitation on the Au array, and the EF decreases with off-resonant excitations. However, for Pt nanodisks the experimental EF is much smaller ($\sim 10^2$) and not sensitive to excitation wavelength. Electric field intensities calculated in Au and Pt nanoparticles using the discrete dipole approximation (DDA) with a dielectric function including or excluding interband transitions allowed us to explain the SERS EF differences at different excitation wavelengths. The observed SERS insensitivity to excitation wavelength in Pt was explained using Fano interference between the free plasmon electrons and continuum interband transitions. The importance of Fano interference was explored analytically in the electrostatic limit by varying the contribution from the interband transitions.

1. Introduction

When subjected to electromagnetic radiation, metal nanostructures support coherent free-electron oscillations. These localized surface plasmon resonances (LSPRs) have been intensively investigated over the last two decades. LSPR allows one to couple electromagnetic energy into nanoscale dimensions with strong field confinement and enhancement.[3] The LSPRs and, consequently, the local electromagnetic field can be tuned by controlling the geometry, composition, and surrounding dielectric of the metal nanostructures.[4−9] This enhanced local field can then be used to amplify emissive processes, for example, to increase the molecular optical cross-section in surface-enhanced Raman spectroscopy (SERS)[10−12] or to enhance nonlinear light generation as in high-order harmonic generation.[13,14] In addition, LSPR enables sensing applications due to its sensitivity to the dielectric properties of the surroundings and optoelectronic applications due to its ability to propagate information by particle−particle coupling.[15−20]

The parallel development of advanced analytical techniques and electrodynamics simulations has enabled a better understanding of LSPR and its effects.[21−25] However, most experimental and theoretical studies have been performed on noble metals, like Au and Ag.[8,26−32] In contrast, applications of LSPR to Pt nanoparticles remain relatively unexplored.[33−37] The location of the Pt nanoparticle's LSPR in the UV makes them much more difficult to probe because of the strong absorption of light by silica and most solvents in this wavelength range.[38] Some initial studies on Pt and Pt−Ag nanoparticles show that their LSPR can be tuned across a large range, from ultraviolet to infrared wavelengths,[39−41] and they are potentially SERS active in this wide range of the electromagnetic spectrum.[33,36,37,42] However, SERS studies on electrochemically roughened Pt electrodes show that the SERS enhancement factor (EF) for Pt is very weak and much lower than those for Au and Ag; the weakness in SERS EF for Pt deserves a better understanding.[34,36]

Fano interferences[43]—characterized by an asymmetric line shape arising from the interaction of a discrete state with a continuum—are commonly found in atomic and solid state structures,[44,45] but there are few examples of the phenomena in plasmonic systems.[46−49] Fano interference has been recently reported in a symmetry-breaking metallic nanostructure.[46] Besides this extrinsic Fano interference, intrinsic Fano interference involving the free and bound electron response of the metal has been shown to play a crucial role in determine the spectral shape of LSPR in Pd particles.[49]

In this work we will show that the Fano interferences in Pt metal nanoparticles not only modify the LSPR line shape but also reduce the enhanced electric field outside the nanoparticles and weaken the surface enhanced spectroscopy performance. Here we present a systematic comparison of the SERS response of Au and Pt with resonant and off-resonant excitations on a long-range ordered array of nanodisks. The observed differences in the SERS EF with excitation wavelength are explained on the basis of the extinction cross sections of the sample and originate from the Fano interference between plasmon electrons and interband transitions in Au and Pt. Both a pure Drude dielectric function and an experimental dielectric function were used in the discrete dipole approximation (DDA) to calculate the LSPR and the confined local electric fields and therefore allow us to indentify the effects of Fano interference. To understand further the importance of Fano interference, we analytically explored the extinction and electric field enhancements in the electrostatic limit.

* Author to whom correspondence should be addressed. Electronic mail: junhuang@psu.edu.
[†] Department of Physics.
[‡] Department of Engineering Science and Mechanics.
[§] Department of Chemistry.
[∥] Department of Materials Science and Engineering.

10.1021/jp105276w © 2010 American Chemical Society
Published on Web 09/03/2010

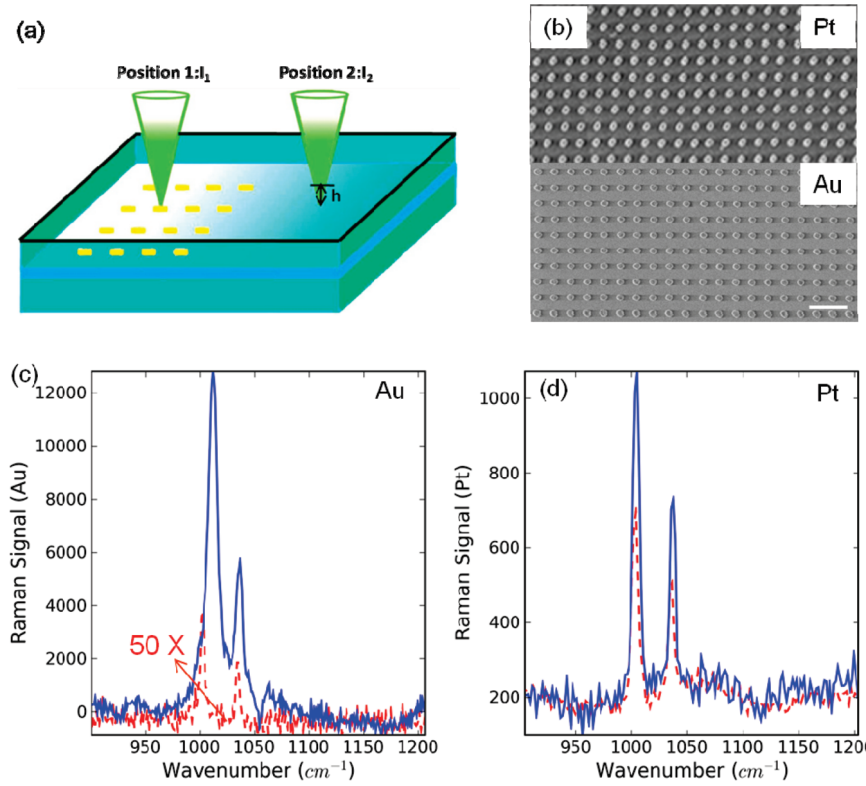

Figure 1. (a) Schematic showing the SERS measurement system. (b) Representative SEM image of Pt and Au nanodisk arrays fabricated using electron beam lithography. Scale bar represents 600 nm. Raman spectra of pyridine on (c) Au substrate with 647 nm excitation and (d) Pt substrate with 488 nm excitation, focused on position 2 (dashed lines) and position 1 (solid lines). The Raman spectrum of pyridine on Au substrate focused on position 2 is magnified by 50×.

2. Experimental Details

Nanodisk arrays were fabricated using e-beam lithography (EBL) on quartz slides. Slides were first cleaned chemically in standard "piranha" solution (1:3 30% H_2O_2: H_2SO_4) at 80 °C for 30 min, followed by ultrapure (18.00 MΩ cm) water rinse. [**Caution!** *Piranha solution is very dangerous, with the majority of its components acidic and highly corrosive. It must be handled extremely carefully.*] Slides were later sonicated in 5:1:1 H_2O/NH_4OH/30% H_2O_2 for 30 min, followed by rinsing with large amounts of ultrapure water. Following standard procedures for e-beam lithography,[50] 120 nm e-beam resist ZEP 520A (ZEON Corp. Japan) was spun onto freshly prepared slides and 10 nm of Au, as an electron conductive layer, was vacuum deposited prior to exposure in the EBL system. After exposure, the Au film was removed in Au Etchant TFA (Transene) for 30 s; the patterns were obtained by developing the sample in *n*-amyl acetate (Sigma Aldrich) at 20 °C for 3 min, followed by immersion into methyl isobutyl ketone (MIBK)/2-propanol (IPA) = 8:1 solvent for 30 s and rinsing in IPA for 30 s. After descum in an O_2 plasma etch (PLASMATHERM 720 RIE), Au and Pt were deposited using e-beam evaporation (K. J. Lesker PVD 75) over the pattern. A thin Cr layer was added to improve adhesion for Au nanodisks. Finally, highly order Au and Pt nanodisk arrays (Figure 1b) with diameter ∼120 nm, height ∼30 nm, and period ∼300 nm (dimensions obtained from the SEM and AFM measurements) were obtained by lifting off the resist in *N*,*N*-dimethylacetamide (Sigma Aldrich) solution at 60 °C.

Extinction spectra of nanodisk arrays or a SERS substrate were measured using a UV−vis−NIR double beam spectrometer (Perkin-Elmer Lambda 950). The beams at both the sample and reference positions were ∼2 mm in diameter; spectra were collected at normal incidence with unpolarized light. The SERS substrate with a particle area of 4 mm × 4 mm and a clean quartz substrate were placed, respectively, in the sample and reference beams, so the absorption from the quartz substrate was excluded in the measured spectra.

The experimental SERS EF was collected using an optical cell containing the SERS substrate (Figure 1a) covered with 0.01 M pyridine (EMD) in 0.1 M KCl solution (EMD). The SERS substrate was preincubated in pure pyridine solution for one day before transferring into the chemical cell to ensure monolayer coverage. A microscope coverslip was added over the top as a thin window in such a way that the cell was completely filled with pyridine solution. Raman spectra (backscattering geometry) were taken using a Renishaw Invia MicroRaman spectrometer with a computer-controlled microscope stage, a cooled CCD detector, and an argon ion laser. The laser radiation was focused onto the plane of the substrate using a 50× objective; the laser spot was about 1 μm in diameter. To obtain the EF for pyridine on Au and Pt arrays, the Raman spectra of pyridine were collected from two focal positions on the substrate, as shown in Figure 1a. The beam positions were reached by a simple horizontal translation of the microscope stage between the portion of the substrate with the SERS active array, where the backscattered Raman intensity is $I_1 = I_{SERS} + I_{solution}$, to a second nearby location on the glass substrate, where no array is present and where the intensity is $I_2 = I_{solution}$. The contribution to I_1 contains a SERS spectrum (I_{SERS}) and a contribution from pyridine in solution in the objective depth of field h above the substrate ($I_{solution}$). The SERS signal (I_{SERS}) stems from molecules in close proximity to the metal particle surface, primarily from those molecules bound to the metal particle surface. This was obtained by computing the Raman intensity difference $I_{SERS} = \Delta I = I_1 - I_2$. To establish

TABLE 1: SERS Enhancement Factor for Au and Pt

excitation wavelength (nm)	Au enhancement factor	Pt enhancement factor
488 (2.55 eV)	2×10^3	2×10^2
514 (2.42 eV)	3×10^3	2×10^2
647 (1.91 eV)	1×10^6	4×10^2

the EF, another measurement was done in pure pyridine liquid using a glass substrate with no nanoparticles and the same spectrometer parameters, giving I_{liquid}, the Raman intensity of pure pyridine liquid. To conservatively estimate the SERS EF, the volume of pure pyridine is approximated by a cylinder whose diameter d (~1 um) is related to the focused spot size of the laser on the substrate surface and whose height h (~45 μm) is the depth of field of the objective and was measured by translating the substrate a distance h away from the objective until the Raman signal from pyridine liquid reaches a maximum. The estimate for the pyridine volume is $V \sim \pi(d/2)^2h$. The number of molecules contributed to I_{liquid} is then $N_{liquid} \sim \rho VA/M$, where ρ is the density of the liquid (0.9819 g/cm^3), M is the molecular weight (79.1 g mol^{-1}), and A is Avogadro's constant. The number of molecules contributed to I_{SERS} was estimated from $N_{SERS} = N_{cyl}S/\sigma$, where N_{cyl} is the number of Au or Pt nanodisks in the focal spot, which can be obtained from the laser focus spot size, d, and the particle density, S is the top and side surface area of one nanodisk ($S \sim 22\,619$ nm^2) and σ is the average surface area occupied by a pyridine molecule, $\sigma = 0.254$ nm^2. This value is the average of experimentally determined ocupation areas of pyridine adsorbed at a smooth Pt electrode (0.243 nm^2),[51] an Hg electrode (0.25 nm^2),[52] and a Au electrode (0.27 nm^2),[53] respectively.

3. Results and Discussion

The SERS EF can be written as,

$$\mathrm{EF} = (I_{SERS}/N_{SERS})/(I_{liquid}/N_{liquid}), \quad (1)$$

where $I_{SERS} = I_1 - I_2$[35] (cf. Figure 1a). For high concentration, pyridine prefers vertically oriented adsorption, bonded to the nanodisk surface through the electron lone pair on the nitrogen atom.[54] We assume that a monolayer of pyridine is formed on the nanodisk surface after incubation. The enhanced electromagnetic fields surrounding a nanoparticle drops off quickly as one moves away from the particle surface,[24] covering about only one monolayer of vertically oriented pyridine molecules. Raman spectra of pyridine collected by a small translation of the microscope stage between position 1 and 2 are shown in Figure 1, with 647 nm excitation for Au (c) and with 488 nm excitation for Pt (d). The scattering background from the metal arrays and quartz substrate and signals from the water solution were subtracted from the displayed spectra. A typical Raman spectrum of pyridine on an Au nanoparticle substrate is available in the Supporting Information. The SERS spectrum of pyridine exhibits two strong peaks, the ring breathing mode at about 1009 cm^{-1}, and the symmetric ring deformation mode at about 1035 cm^{-1}, compared to 991 and 1030 cm^{-1} for liquid pyridine, respectively. The changes in peak positions are attributed to the water environment and interaction with metal particles.[12] SERS EF results for Au and Pt at three excitation wavelengths, 488 nm (2.55 eV), 514 nm (2.42 eV), and 647 nm (1.91 eV) calculated according to eq 1 based on the strongest peak at 1009 cm^{-1} are tabulated in Table 1.

It is well established that the SERS EF for Ag and Au nanoparticles closely follows the plasmonic extinction resonance.[55,56] We therefore examined the extinction spectra (extinction = absorption + scattering) of the Au and Pt nanodisk arrays. For the very small particles studied here, absorption accounts for the major part of extinction. In Figure 2, we display the experimentally measured extinction Q_A/ω vs photon energies for the SERS substrates, where $Q_A = \log_{10}(1/T)$ and T is the transmittance. The reason we plot Q_A/ω is that it is linearly proportional to the imaginary part of the dipole polarizability, that is, $Q_A/\omega \propto \mathrm{Im}[\alpha(\omega)]$. The peak in the Q_A/ω is identified as the LSPR, and its position is found around 2.0 and 2.7 eV for Au and Pt, respectively, which is consistent with values reported in the literature.[40] The displayed curves were normalized to the extinction of Au. For the same particle size and density, the experimental measured extinction cross-section of Pt is about half that of Au.

By locating the excitation laser wavelength on the extinction spectra, we found that SERS EF for Au follows the extinction spectrum and has a maximum measured EF at 1.91 eV excitation, which closely aligns to the Au LSPR (cf. Figure 2). For off-resonant excitations at 2.42 and 2.55 eV, the EF drops by about 3 orders of magnitude. In contrast, the SERS EF for Pt is largely unaffected by changes in the excitation wavelength and thus do not follow the plasmon extinction spectrum. Moreover, EF for Pt is significantly smaller than for Au. For Au the EF on resonance is about 10^6, consistent with other work.[10] The EFs for Pt at different excitation wavelengths all have similar magnitudes, ~10^2, in agreement with that obtained for Au@Pt core−shell particles.[34] It is well-known that the EF is determined by not only the LSPR peak but also its line width.[57] Therefore, to understand the different EF behaviors between Au and Pt, we further examined the line shape of the extinction spectra. The line width of Pt, 0.6 eV, is about 3 times that of Au, 0.2 eV. Moreover, the extinction spectrum for Pt is more asymmetric than that of Au. Similar asymmetric and broad extinction spectra have been reported for Pd, which was attributed to Fano interference between the free plasmon electrons and the extended interband continuum arising from transitions between sp, d, and hybridized bands around the Fermi energy.[49] To understand if the difference in the SERS EF on Au and Pt is caused by Fano interference,[43] we characterized the extinction spectra using the Fano line-shape function given by:

$$F(\omega) = A\frac{\left[q + \frac{\omega - \omega_0}{\Gamma}\right]^2}{\left[1 + \left(\frac{\omega - \omega_0}{\Gamma}\right)^2\right]} = A\left[\frac{(q^2 - 1)\Gamma^2}{(\omega - \omega_0)^2 + \Gamma^2} + 1 + \frac{2q\Gamma(\omega - \omega_0)}{(\omega - \omega_0)^2 + \Gamma^2}\right] \quad (2)$$

Here, ω_0 and Γ are the effective resonant position and line width, respectively, A is a constant, and q is inversely proportional to the degree of line-shape asymmetry, and thus we quantify the strength of the Fano interference by $1/q$. Equation 2 is the full response function of a discrete resonance coupled to a continuum and is composed of three constituents: a symmetric Lorentzian term due to discrete resonance of free electrons, a constant term due to the continuum of interband transitions, and an interference term between the discrete resonance and the continuum. Our experimental data is well described by a Fano line shape, as

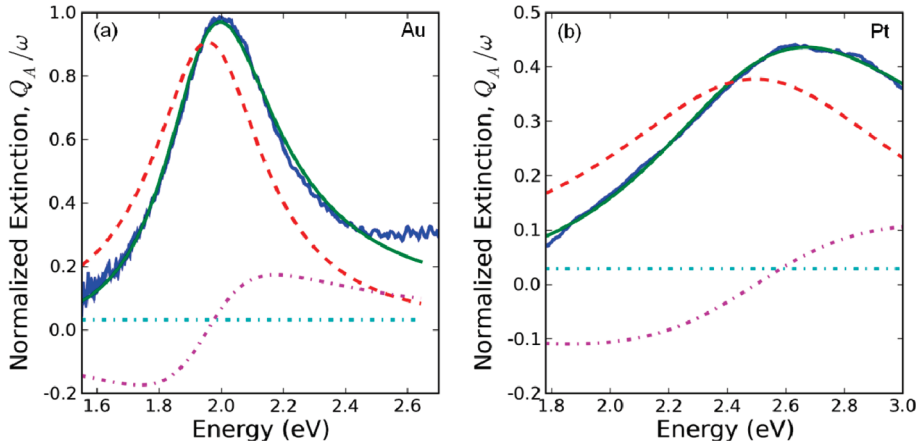

Figure 2. Decomposition of the experimentally measured extinction Q_A/ω of Au (a) and Pt (b) (bold lines) nanodisks into a Fano line shape. The components of the Fano line shape include a Lorentzian term (dashed lines), non-Lorentzian term (dotted lines), and a constant background term (dash-dotted lines) for both Au and Pt.

seen in Figure 2. From the fit we find that the asymmetry parameter for Pt is $1/q = 0.33$, and that of Au is $1/q = 0.13$. The value of q for Pt is comparable with that for Pd,[49] which is expected since the two metals are similar. The larger asymmetry of the Pt extinction spectrum compared with that for Au indicates that interference between plasmon and interband transitions in Pt plays an important role.

To understand the effect of the Fano interference on the SERS, we need to consider the EF in more detail. The SERS enhancement mechanism can roughly be understood in terms of three mechanisms:[58−60] (a) an electromagnetic mechanism (EM) due to resonance of the incident beam with the plasmon of the metal surface, (b) a charge transfer (CT) mechanism due to resonance of the incident beam with an excitation from the metal to the adsorbate, and (c) an enhancement due to nonresonant interactions between the surface and the adsorbate (CHEM). Mechanisms (b) and (c) are generally combined as a chemical mechanism.

These three mechanisms act in concert to give the total enhancement in SERS. The strongest enhancement is the EM due to the strong local field near the metal surface when the plasmons are excited. The SERS intensities scale roughly with the local field as $|E_{loc}/E_{inc}|^4$, where E_{loc} is the electric field at the surface and E_{inc} is the incident electric field,[23] and thus is highly sensitive to the local field. The CT and CHEM mechanisms are typically weaker, on the order of 10−1000×. The CHEM mechanism is largely independent of the incident light. In the CT mechanism the enhancement scales as $1/\Gamma^4$, where Γ is the half-width of the electronic transition. For metal−molecule CT transitions relevant for SERS, Γ can easily be on the order of 0.5−1 eV. Furthermore, due to the broader line shape width in the extinction spectra of Pt compared to Au we expect the CT mechanism to be less important for Pt. Therefore, we focus on understanding how Fano interference influences the EM.

To do this, we simulated the extinction efficiency and electric field (E-field) intensity outside a single Au or Pt nanodisk for various excitation wavelengths using the discrete dipole approximation (DDA). We used the DDSCAT program (version 6.1) by Draine and Flatau.[61] In the simulations the nanoparticle was represented by a nanodisk with a diameter of 120 nm and a height of 30 nm. The total number of dipoles in the simulations was 12 640. A linear polarized plane wave provided the excitation. For the dielectric constant needed in the DDA simulations we used the experimentally determined dielectric constant[1,2] or a Drude−Lorentz model. The complex dielectric function $\varepsilon(\omega)$ can be expressed as[62,63] $\varepsilon(\omega) = \varepsilon_F(\omega) + \varepsilon_I(\omega)$, which separates intraband effects (free electrons) from interband effects (so-called bound electrons). The intraband part $\varepsilon_F(\omega)$ of the dielectric function can be described by the well-known Drude model:[64,65]

$$\varepsilon_F(\omega) = 1 - \frac{f_0{\omega_p}^2}{\omega(\omega - i\Gamma_0)} \tag{3}$$

where ω_p is the plasma frequency associated with intraband transitions with oscillator strength f_0 and damping constant Γ_0. The interband part of the dielectric function $\varepsilon_I(\omega)$ can be approximated by a simple semiquantum model resembling the Lorentz model for insulators:

$$\varepsilon_I(\omega) = \sum_{j=1}^{k} \frac{f_j{\omega_p}^2}{({\omega_j}^2 - \omega^2) + i\omega\Gamma_j} \tag{4}$$

where k is the number of oscillators, each with frequency ω_j, strength f_j, and lifetime $1/\Gamma_j$. The parameters for the combined Drude−Lorentz model were taken from ref 57 and provide a good fit to the experimental data,[66] as shown in Figure 3. For Au, the interband transition threshold is about 2.4 eV and thus above the plasmon resonance,[67] while Pt shows a large continuum of interband transitions extending far below the visible wavelengths, which gives rise to the large Fano interference with the free electrons.

The calculated extinction spectra using the experimental dielectric constant (Figure 4a,b) matches the experimentally measured ones (cf. Figure 2). The total E-field intensity on the particle for various excitation wavelengths (normalized to the maximum E-field on the particle for resonant excitation) was used to represent the average E-field enhancement by the particle. Since strong E-field enhancement only occurs close to the particle surface, the total E-field on the particle reflects the averaged strength of E-field contribution to EM enhancement. Figure 4d illustrates the typical E-field intensity distribution, $|E_{loc}|^2$, near the surface of an Au nanodisk calculated at a resonant excitation of 615 nm. The average E-field enhancement for different excitation wavelength is shown in Figure 4a,b for Au and Pt nanodisks, respectively. We see that the E-field enhancement for Au follows closely the LSPR with a maximum

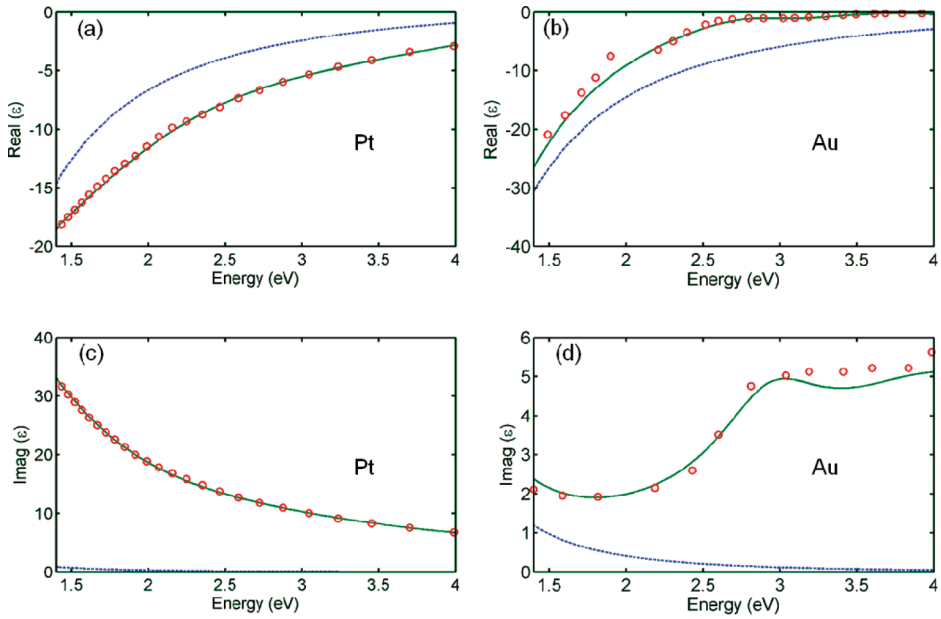

Figure 3. Drude−Lorentz model (solid line) fits to experimentally measured dielectric function (dots) of Pt[1] and Au.[2] The Drude component is shown as a dashed line. In stark contrast to Au, Pt exhibits a large continuum of interband transitions.

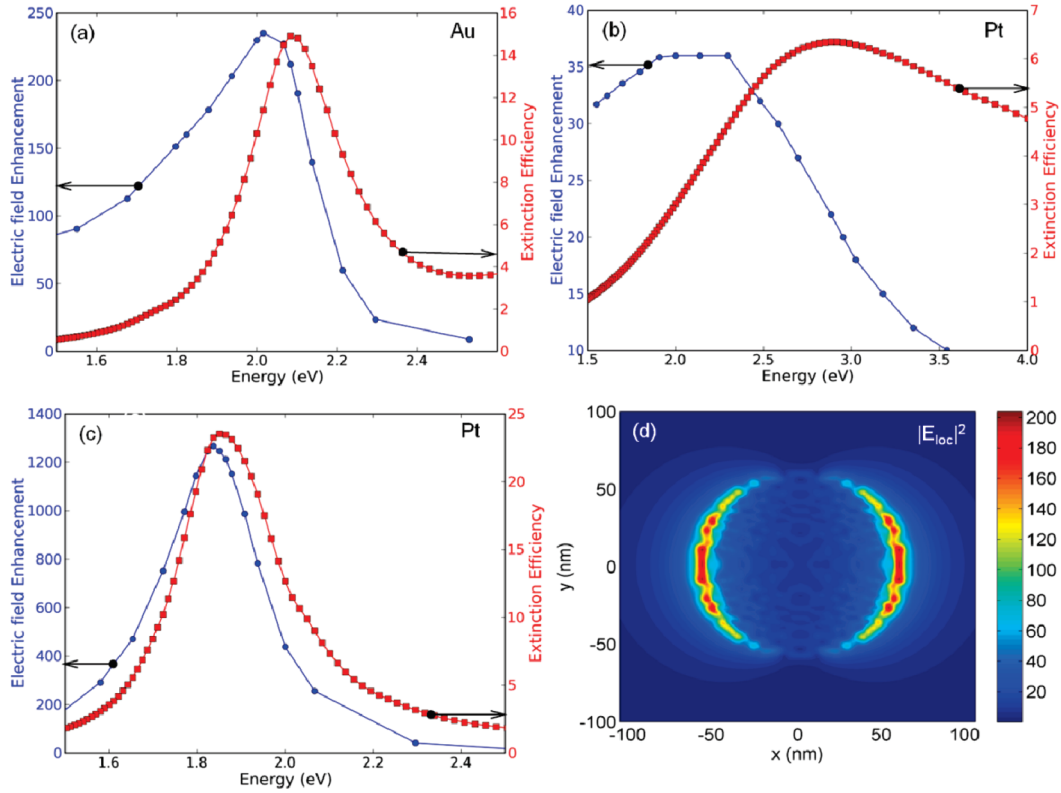

Figure 4. DDA simulation of electric field enhancement and extinction efficiency for Au (a) and Pt (b) using the experimentally determined dielectric constant. (c) DDA simulation of electric field enhancement and extinction efficiency for Pt using only a Drude model for the dielectric constant. (d) Typical electric field intensity distribution $|E_{loc}|^2$ near the top of an Au nanodisk at 615 nm wavelength.

enhancement in *E*-field of ∼240 at resonance, which corresponds to an EM enhancement of $\sim 10^5$. In contrast, the *E*-field enhancement for Pt is small and relatively uniform over a wide wavelength range with a maximum of ∼36, which would yield an EM enhancement of $\sim 10^3$. Thus, the EM enhancement estimated from the DDA simulation agrees reasonably with the measured values (Table 1), given the complexity in the SERS enhancement mechanism and the approximations used in the simulation.

To understand the influence of interband transitions, we repeated the calculation for Pt without interband contributions by using a purely Drude model for the dielectric constant when the extinction efficiency and the *E*-field enhancement or $|E_{loc}|^2$ were calculated for Pt. In the absence of the continuum interband transitions, $|E_{loc}|^2$ is extremely large and shows the same wavelength dependence as the plasmon resonance, as shown in Figure 4c. Thus we conclude that Fano interference between plasmon electrons and interband transition modulates the

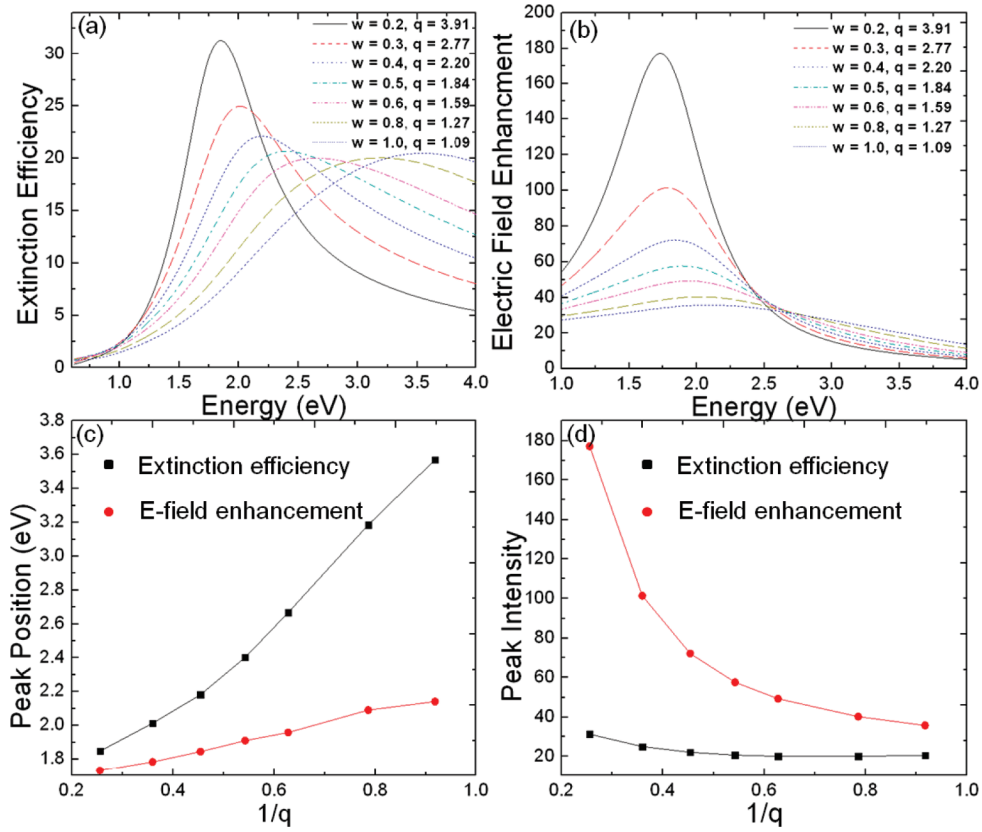

Figure 5. Plot of extinction efficiency (a) and electric field enhancement (b) for Pt calculated analytically in the electrostatic limit. The contribution of interband transition to the Drude−Lorentz dielectric determines the Fano interference strength, $1/q$. (c) Peak positions of extinction efficiency (black squares) and electric field enhancement (red dots) for different Fano interference strengths. (d) Peak intensity of extinction efficiency (black squares) and electric field enhancement (red dots) for different Fano interference strengths.

electromagnetic response of Pt, producing a very large damping, thereby lowering the enhancement in the *E*-field and altering the wavelength dependence of the *E*-field enhancement so that it does not follow the LSPR.

The origin of the Fano interference on the EM enhancement can be understood by considering a molecule adsorbed on an oblate ellipsoid under an external laser field E_L of frequency ω_L. If the dimension of the ellipsoid is much smaller than the wavelength, the problem can be solved in an electrostatic approximation. We replace the ellipsoid by an effective point dipole of magnitude $\mu = \alpha_E E_L$[68] where

$$\alpha_E(\omega) = V\frac{\varepsilon - \varepsilon_m}{3\varepsilon_m + 3L(\varepsilon - \varepsilon_m)} \quad (5)$$

Equation 5 describes the polarizability components along the long axis of the ellipsoid. At resonance, the induced dipolar field of the ellipsoid is very large and produces a large molecular dipole moment μ_M oscillating at the Stokes frequency ω_S: $\mu_M(\omega_S) = 2\alpha_R\alpha_E(\omega_L)E_L/r^3$.[56] Here α_R is the Raman polarizability and r is the distance from the center of the ellipsoid to the molecule. The field of the molecular dipole in turn polarizes the ellipsoid to produce an ellipsoid dipole at the Stokes frequency, $\mu_E = 2\alpha_E(\omega_S)\,\mu_M(\omega_S)E_L/r^3$, which is larger than the usual Raman molecular dipole by the factor $f = (4/(r^3)^2)\alpha_E(\omega_L)\,\alpha_E(\omega_S) \approx (4/(r^3)^2)\alpha_E(\omega_L)^2$ since the Stokes frequency is usually very close to the laser frequency.

The enhancement in the electric field intensity, F, at the surface of the ellipsoid is $F = |f| = (4/(r^3)^2)|\alpha_E(\omega_L)|^2$, and the net enhancement of the Raman intensity is $F^2 = (16/(r^3)^4)|\alpha_E(\omega_L)|^4$. By simply investigating the effects of interband transitions on the polarizability $\alpha_E(\omega)$, we can understand the differences in the wavelength-dependent electric field enhancement behavior in Au and Pt. The polarizability of an ellipsoid (eq 5) can be rearranged to yield[49] $\alpha_E(\omega) = (V/3L)[\alpha_F(\omega) + \alpha_I(\omega) - \alpha_F(\omega)\,\alpha_I(\omega)]$ where $\alpha_F(\omega)$ is the free electron response and $\alpha_I(\omega)$ is the pure interband response. The free electron response is $\alpha_F(\omega) = \omega_{LSP}^2/(\omega_{LSP}^2 - \omega^2 - i\gamma\omega)$, where $\omega_{LSP}^2 = \omega_p^2/B$ and the pure interband response is $\alpha_I(\omega) = (\varepsilon_I - \varepsilon_m)/B$ where ε_I is the complex interband contribution to the dielectric function, ε_m is the dielectric constant of the medium and $B = (1/L - 1)\varepsilon_m - \varepsilon_I$. The electric field enhancement is therefore $F = |f| = |f_F + f_I + f_F f_I + 2\alpha_F\cdot\alpha_I(1 - \alpha_F - \alpha_I)|$, where f_F is the enhancement in the electric field due to the free electron response, f_I is the enhancement in the electric field due to the pure interband response, and the remainder are interference terms. To understand the role of interband transitions in the extinction and the electric field enhancement for Pt, we changed the weight fraction (w) of the Lorentz part in the Drude−Lorentz model as $\varepsilon(\omega) = \varepsilon_F(\omega) + w \times \varepsilon_I(\omega)$. Figure 5a shows the extinction efficiencies for various weighting factions and the corresponding fitting parameter q in the Fano line-shape function. A larger contribution from interband transitions gives a smaller q, a stronger Fano interference ($1/q$), and therefore a much more asymmetric spectrum. The calculated *E*-field enhancement is shown in Figure 5b with different weight fractions. As Fano interference becomes stronger, the separation between *E*-field enhancement peaks and extinction resonance peaks becomes larger. *E*-field enhancement no longer follows

the extinction spectrum (Figure 5c). As a result, we observe that the SERS EF for Pt is insensitive to the extinction spectrum. Moreover, stronger Fano interference also results in much a weaker extinction and *E*-field enhancement (Figure 5d), and consequently there is much weak SERS EF ($\sim 10^2$) in Pt. The analytical model qualitatively explains the experimentally measured SERS EF in Pt.

4. Conclusions

The different plasmonic behaviors of Au and Pt nanodisks and consequently their different SERS EF as a function of excitation wavelength were explained by Fano interference between free plasmon electrons and interband transitions. Compared to that of Au, the extinction spectrum of Pt is broader and more asymmetric. A large experimental Raman cross-section enhancement factor (EF) of $\sim 10^6$ was obtained with 647 nm resonant excitation on the Au array with the EF decreasing significantly off-resonance. In contrast, the SERS EF for Pt array is much smaller, $\sim 10^2$, and not particularly sensitive to the excitation wavelength. Discrete dipole approximation simulations with a Drude dielectric constant or an experimental dielectric constant attribute the low EF and insensitivity to excitation wavelength in Pt to Fano interference between free electrons and continuum interband transitions. An analytical model reveals that increasing the Fano interference leads to a significantly weaker *E*-field enhancement and different wavelength dependence from that found for the extinction spectrum.

Acknowledgment. We gratefully acknowledge the financial support from Air Force Office of Scientific Research (AFOSR), National Science Foundation (NSF), U.S. Department of Agriculture (USDA), and the Penn State Center for Nanoscale Science (MRSEC). Components of this work were conducted at the Penn State node of the NSF-funded National Nanotechnology Infrastructure Network (NNIN).

Supporting Information Available: Figure of typical Raman spectrum of pyridine on a Au nanodisk. This material is available free of charge via the Internet at http://pubs.acs.org.

References and Notes

(1) Weaver, J. H. *Phys. Rev. B* **1975**, *11*, 1416.
(2) Theye, M. L. *Phys. Rev. B: Solid State* **1970**, *2*, 3060.
(3) Maier, S. A.; Atwater, H. A. *J. Appl. Phys.* **2005**, *98*.
(4) Zheng, Y. B.; Huang, T. J.; Desai, A. Y.; Wang, S. J.; Tan, L. K.; Gao, H.; Huan, A. C. H. *Appl. Phys. Lett.* **2007**, *90*.
(5) Zheng, Y. B.; Jensen, L.; Yan, W.; Walker, T. R.; Juluri, B. K.; Jensen, L.; Huang, T. J. *J. Phys. Chem. C* **2009**, *113*, 7019.
(6) Wiley, B.; Sun, Y. G.; Chen, J. Y.; Cang, H.; Li, Z. Y.; Li, X. D.; Xia, Y. N. *MRS Bull.* **2005**, *30*, 356.
(7) Zheng, Y. B.; Yang, Y. W.; Jensen, L.; Fang, L.; Juluri, B. K.; Flood, A. H.; Weiss, P. S.; Stoddart, J. F.; Huang, T. J. *Nano Lett.* **2009**, *9*, 819.
(8) Halas, N. *MRS Bull.* **2005**, *30*, 362.
(9) Hsiao, V. K. S.; Zheng, Y. B.; Juluri, B. K.; Huang, T. J. *Adv. Mater.* **2008**, *20*, 3528.
(10) Haynes, C. L.; McFarland, A. D.; Van Duyne, R. P. *Anal. Chem.* **2005**, *77*, 338A.
(11) Campion, A.; Kambhampati, P. *Chem. Soc. Rev.* **1998**, *27*, 241.
(12) Fleischm, M.; Hendra, P. J.; Mcquilla, Aj. *Chem. Phys. Lett.* **1974**, *26*, 163.
(13) Bloember, N.; Chang, R. K.; Jha, S. S.; Lee, C. H. *Phys. Rev.* **1968**, *174*, 813.
(14) Bozhevolnyi, S. I.; Beermann, J.; Coello, V. *Phys. Rev. Lett.* **2003**, *90*.
(15) Lal, S.; Link, S.; Halas, N. J. *Nat. Photonics* **2007**, *1*, 641.
(16) Anker, J. N.; Hall, W. P.; Lyandres, O.; Shah, N. C.; Zhao, J.; Van Duyne, R. P. *Nat. Mater.* **2008**, *7*, 442.
(17) Zhao, J.; Zhang, X. Y.; Yonzon, C. R.; Haes, A. J.; Van Duyne, R. P. *Nanomedicine* **2006**, *1*, 219.
(18) Roca, M.; Haes, A. J. *Nanomedicine* **2008**, *3*, 555.
(19) Dmitriev, A.; Hagglund, C.; Chen, S.; Fredriksson, H.; Pakizeh, T.; Kall, M.; Sutherland, D. S. *Nano Lett.* **2008**, *8*, 3893.
(20) Willets, K. A.; Van Duyne, R. P. *Annu. Rev. Phys. Chem.* **2007**, *58*, 267.
(21) Juluri, B. K.; Lu, M. Q.; Zheng, Y. B.; Huang, T. J.; Jensen, L. *J. Phys. Chem. C* **2009**, *113*, 18499.
(22) Kelly, K. L.; Coronado, E.; Zhao, L. L.; Schatz, G. C. *J. Phys. Chem. B* **2003**, *107*, 668.
(23) Jensen, L.; Aikens, C. M.; Schatz, G. C. *Chem. Soc. Rev.* **2008**, *37*, 1061.
(24) Haes, A. J.; Haynes, C. L.; McFarland, A. D.; Schatz, G. C.; Van Duyne, R. R.; Zou, S. L. *MRS Bull.* **2005**, *30*, 368.
(25) Wu, D. Y.; Li, J. F.; Ren, B.; Tian, Z. Q. *Chem. Soc. Rev.* **2008**, *37*, 1025.
(26) Zheng, Y. B.; Huang, T. J. *J. Assoc. Lab. Autom.* **2008**, *13*, 215.
(27) Juluri, B. K.; Zheng, Y. B.; Ahmed, D.; Jensen, L.; Huang, T. J. *J. Phys. Chem. C* **2008**, *112*, 7309.
(28) Ni, W. H.; Chen, H. J.; Kou, X. S.; Yeung, M. H.; Wang, J. F. *J. Phys. Chem. C* **2008**, *112*, 8105.
(29) Kneipp, K.; Wang, Y.; Kneipp, H.; Perelman, L. T.; Itzkan, I.; Dasari, R.; Feld, M. S. *Phys. Rev. Lett.* **1997**, *78*, 1667.
(30) Wu, D. Y.; Liu, X. M.; Duan, S.; Xu, X.; Ren, B.; Lin, S. H.; Tian, Z. Q. *J. Phys. Chem. C* **2008**, *112*, 4195.
(31) Xia, Y. N.; Halas, N. J. *MRS Bull.* **2005**, *30*, 338.
(32) Zheng, Y. B.; Juluri, B. K.; Mao, X. L.; Walker, T. R.; Huang, T. J. *J. Appl. Phys.* **2008**, *103*.
(33) Tian, Z. Q.; Yang, Z. L.; Ren, B.; Wu, D. Y. *Top. Appl. Phys.* **2006**, *103*, 125.
(34) Cui, L.; Wang, A.; Wu, D. Y.; Ren, B.; Tian, Z. Q. *J. Phys. Chem. C* **2008**, *112*, 17618.
(35) Cai, W. B.; Ren, B.; Li, X. Q.; She, C. X.; Liu, F. M.; Cai, X. W.; Tian, Z. Q. *Surf. Sci.* **1998**, *406*, 9.
(36) Ren, B.; Huang, Q. J.; Cai, W. B.; Mao, B. W.; Liu, F. M.; Tian, Z. Q. *J. Electroanal. Chem.* **1996**, *415*, 175.
(37) Kim, N. H.; Kim, K. *J. Raman Spectrosc.* **2005**, *36*, 623.
(38) Creighton, J. A.; Eadon, D. G. *J. Chem. Soc., Faraday Trans.* **1991**, *87*, 3881.
(39) Langhammer, C.; Yuan, Z.; Zoric, I.; Kasemo, B. *Nano Lett.* **2006**, *6*, 833.
(40) Langhammer, C.; Kasemo, B.; Zoric, I. *J. Chem. Phys.* **2007**, *126*.
(41) Chen, J. Y.; Wiley, B.; McLellan, J.; Xiong, Y. J.; Li, Z. Y.; Xia, Y. N. *Nano Lett.* **2005**, *5*, 2058.
(42) Tian, Z. Q.; Ren, B.; Wu, D. Y. *J. Phys. Chem. B* **2002**, *106*, 9463.
(43) Fano, U. *Phys. Rev.* **1961**, *1*, 1866.
(44) Gores, J.; Goldhaber-Gordon, D.; Heemeyer, S.; Kastner, M. A.; Shtrikman, H.; Mahalu, D.; Meirav, U. *Phys. Rev. B* **2000**, *62*, 2188.
(45) Faist, J.; Capasso, F.; Sirtori, C.; West, K. W.; Pfeiffer, L. N. *Nature* **1997**, *390*, 589.
(46) Hao, F.; Sonnefraud, Y.; Van Dorpe, P.; Maier, S. A.; Halas, N. J.; Nordlander, P. *Nano Lett* **2008**, *8*, 3983.
(47) Tribelsky, M. I.; Flach, S.; Miroshnichenko, A. E.; Gorbach, A. V.; Kivshar, Y. S. *Phys. Rev. Lett.* **2008**, *100*.
(48) Verellen, N.; Sonnefraud, Y.; Sobhani, H.; Hao, F.; Moshchalkov, V. V.; Van Dorpe, P.; Nordlander, P.; Maier, S. A. *Nano Lett.* **2009**, *9*, 1663.
(49) Pakizeh, T.; Langhammer, C.; Zoric, I.; Apell, P.; Kall, M. *Nano Lett.* **2009**, *9*, 882.
(50) Haynes, C. L.; McFarland, A. D.; Zhao, L. L.; Van Duyne, R. P.; Schatz, G. C.; Gunnarsson, L.; Prikulis, J.; Kasemo, B.; Kall, M. *J. Phys. Chem. B* **2003**, *107*, 7337.
(51) Gui, Y. P.; Kuwana, T. *J. Electroanal. Chem.* **1987**, *222*, 321.
(52) Conway, B. E.; Mathieso, J. G.; Dhar, H. P. *J. Phys. Chem.* **1974**, *78*, 1226.
(53) Stolberg, L.; Lipkowski, J.; Irish, D. E. *J. Electroanal. Chem.* **1990**, *296*, 171.
(54) Krauskopf, E. K.; Ricejackson, L. M.; Wieckowski, A. *Langmuir* **1990**, *6*, 970.
(55) McFarland, A. D.; Young, M. A.; Dieringer, J. A.; Van Duyne, R. P. *J. Phys. Chem. B* **2005**, *109*, 11279.
(56) Liao, P. F.; Bergman, J. G.; Chemla, D. S.; Wokaun, A.; Melngailis, J.; Hawryluk, A. M.; Economou, N. P. *Chem. Phys. Lett.* **1981**, *82*, 355.
(57) Stietz, F.; Bosbach, J.; Wenzel, T.; Vartanyan, T.; Goldmann, A.; Trager, F. *Phys. Rev. Lett.* **2000**, *84*, 5644.
(58) Jensen, L.; Zhao, L. L.; Schatz, G. C. *J. Phys. Chem. C* **2007**, *111*, 4756.
(59) Lombardi, J. R.; Birke, R. L. *J. Phys. Chem. C* **2008**, *112*, 5605.
(60) Morton, S. M.; Jensen, L. *J. Am. Chem. Soc.* **2009**, *131*, 4090.
(61) Draine, B. T.; Flatau, P. J. http://arxiv.org/abs/astro-ph/0409262, 2004.

(62) Ehrenreich, H.; Philipp, H. R.; Segall, B. *Phys. Rev.* **1963**, *132*, 1918.

(63) Ehrenreich, H.; Sagalyn, P. L.; Philipp, H. R. *Phys. Rev.* **1962**, *128*, 1622.

(64) Markovic, M. I.; Rakic, A. D. *Appl. Opt.* **1990**, *29*, 3479.

(65) Markovic, M. I.; Rakic, A. D. *Opt. Laser Technol.* **1990**, *22*, 394.

(66) Rakic, A. D.; Djurisic, A. B.; Elazar, J. M.; Majewski, M. L. *Appl. Opt.* **1998**, *37*, 5271.

(67) Johnson, P. B.; Christy, R. W. *Phys. Rev. B* **1972**, *6*, 4370.

(68) Bohren, C. F.; Huffman, D. R. *Absorption and Scattering of Light by Small Particles*; John Wiley & Sons: New York, 1983.

JP105276W